Available online at www.sciencedirect.com
ScienceDirect
Trans. Nonferrous Met. Soc. China 27(2017) 1907−1919
Transactions of Nonferrous Metals Society of China
www.tnmsc.cn

Multilayer aluminum composites prepared by rolling of pure and anodized aluminum foils

Milan T. JOVANOVIĆ, Nenad ILIĆ, Ivana CVIJOVIĆ-ALAGIĆ, Vesna MAKSIMOVIĆ, Slavica ZEC

Department of Materials Science, Institute of Nuclear Sciences "Vinča",
University of Belgrade, P. O. Box 522, 11001 Belgrade, Serbia

Received 17 August 2016; accepted 27 January 2017

Abstract: Experimental results on processing, structural and mechanical characterization of a multilayer composite based on commercially pure aluminum foils were presented. A multilayer composite was produced by hot-rolling of anodized and non-anodized aluminum foils alternately sandwiched. In addition, the same process was applied for bonding of non-anodized foils. In both cases, obtained multilayer composites were compact and sound. In order to study composites microstructural evolution and mechanical properties, optical and scanning electron microscopy (SEM), energy dispersive spectrometry (EDS), X-ray diffraction (XRD) analysis, hardness, tensile and three-point flexural tests were performed. Microstructural characterization confirmed that the rod-like particles distributed in parallel rows in the composite aluminum matrix with anodized foils correspond to Al_2O_3. Maximum and minimum peaks of oxygen and aluminum, respectively, suggest that after the final hot-rolling of composite with non-anodized foils, a small amount of coarser particles were formed at boundaries between foils. Hardness, strength, modulus of elasticity and flexural strength of both multilayer composites were much higher than those of pure aluminum, whereas ductility was significantly less. The composite with anodized foils exhibited the highest strength and modulus of elasticity, but lower ductility compared to composite processed from non-anodized foils. Fracture failure corresponded to the change of ductility.
Key words: aluminum foils; anodization; multilayer composite; Al_2O_3 particles; strength; fracture

1 Introduction

Metallic multilayer composites with different component metals have some special advantages in mechanical, electrical and magnetic properties [1−3], which cannot be obtained simply by the counterparts. Many processing methods for multilayer composites, such as physical vapor deposition [4], magnetic sputtering [5], jet-vapor deposition [6] and electro-plating [7] have been reported in the literature. Recently, much attention has been focused on the development of multilayer composites in the form of bulk via deformation processes such as repeated folding and rolling of two or more sheets stacked securely on top of the other, the process called accumulative roll bonding (ARB) [8,9], and repeated extrusion and rolling methods [10]. ARB, regarded as a new kind of severe plastic deformation method, is an efficient way to produce metallic multilayer composites [11−13] with ultra-fine grains and different interface structures [14].

Due to their high corrosion resistance and thermal stability, aluminum and its alloys are popular material choices for structural applications in the aerospace and automotive industries [15−17]. Over the past few years, ARB has been successfully used to produce multilayer structures of different Al-based systems, including Al−Cu [18,19], Al−Zn [20−22], Al−Ni [23], Al−Mg [24,25], Al−Mn [26], Al−Ti [27,28].

The particle reinforced aluminum matrix composites are widely used in aerospace [27], military [29,30] and automotive industries [31] because of their properties such as high specific strength, improved elastic modulus, high wear resistance, high thermal conductivity and excellent corrosion resistance [16−31]. Al_2O_3 particles are the most commonly used reinforcements in aluminum matrix composites and addition of this reinforcement to aluminum alloys has been the subject of several research works [24,31]. In spite of the matrix strengthening and fine grain size which certainly lead to the improvement of mechanical properties, in composites prepared by the conventional

Corresponding author: Ivana CVIJOVIĆ-ALAGIĆ; Tel/Fax: +381-11-3408-224; E-mail: ivanac@vinca.rs
DOI: 10.1016/S1003-6326(17)60215-2

liquid metallurgy route, Al_2O_3 nano-particles as reinforcement often tend to agglomerate even when mechanical stirring is applied before casting [32,33]. The influence of the non-uniform distribution and poor wettability of reinforcing oxides on mechanical and electrical properties of composites is the main drawback of this process [34].

To avoid the problem of agglomeration, fine Al_2O_3 particles were uniformly dispersed between strips of Al1100 and subjected to thirteen cycles of ARB [35]. The excellent distribution of Al_2O_3 particles in the aluminum matrix and the sound bonding between Al_2O_3 particles and the matrix were reported. In another work, fine Al_2O_3 powders with 0.47 μm particle size were dispersed between commercially pure aluminum sheets to produce aluminum-Al_2O_3 composite by ARB [36]. In both works, the strength of composites was significantly increased compared to aluminum used as original raw material. The ARB process coupled with Al_2O_3 particles is applied for manufacturing high-strength and highly-uniform composites as a new technique [37−41].

Many of above mentioned processing routes are usually expensive and their manufacturing parameters are rather difficult to maintain. The objective of this work was an attempt to introduce economical and controllable parameters in processing aluminum matrix reinforced with Al_2O_3. The process involved the formation of thin Al_2O_3 film on commercially pure aluminum foil by anodizing. The bonding between foils was achieved by hot-rolling in order to crush the Al_2O_3 film and disperse it into the aluminum matrix.

2 Experimental

2.1 Material and processing

The commercial household aluminum foils 17 μm thick (technical specification: alloy 8011; temper O; chemical composition (mass fraction, %): 98.73 Al, 0.5 Si, 0.68 Fe, 0.024 Cu, 0.01 Mn, 0.009 Ti, up to 0.15 residual; brand name: Shenzhou Aluminum) were used as a material (referred as "pure aluminum" in the following text) for multilayer composite processing. The chemical composition of the commercial household aluminum foils was specified by the supplier (Jiangsu Shenzhou Aluminum Industry Co., Ltd., China).

Strips with dimensions of 25 mm × 70 mm were cut for anodization which was performed in a 20% water solution of H_2SO_4, with 100 A/m^2 of current density. A round platinum grid was used as a cathode. Anodization was performed at room temperature with duration ranging from 5 to 30 min. Experiments showed that the optimal results were obtained after 20 min of anodization. Such foils together with pure aluminum foils were used for processing of multilayer composites. After anodization, foil was rinsed with water jet, dried with hot air, whereas the upper part of the foil not immersed into the acid was cut. The total number of foils was 100, i.e., 50 anodized and 50 non-anodized foils were alternately packed (designation as A in the further text).

Another "package" of 100 non-anodized foils with the same dimensions as those anodized was also prepared (designation NA). "Packages" were wrapped with wider aluminum foil to prevent the dismount of foils during annealing and hot-rolling.

The binding of foils was performed following the procedures:

1) Foils were wrapped with a wide aluminum foil to prevent the dismount of foils during the first stage of annealing and hot-rolling. The thickness of such a "package" was approximately 3 mm;

2) All annealings were performed using the laboratory furnace in air at 500 °C and duration of the first annealing was 2 h, whereas the temperature of rolls was maintained at 250 °C;

3) Hot rolling (hot rolling procedure was performed using the rolling mill supplied by Albert Mann Engineering Co. Ltd.) to the thickness of "package" up to 3 mm, when the binding started to occur;

4) Intermediate annealing at 500 °C for 15 min;

5) Three passes of hot-rolling up to D_0=2.3 mm thickness (starting thickness);

6) Intermediate annealing at 500 °C for 15 min;

7) Three passes of hot-rolling up to D_1=1.5 mm thickness (between 10% and 15% reduction per pass, and about 35% reduction in total for the first stage);

8) Final annealing at 500 °C for 1 h;

9) Three passes of rolling to the final thickness D_2=0.7 mm of compact material (approximately 15% per pass, and about 50% reduction in total for the second stage).

The total amount of hot deformation, i.e., $(D_0-D_2)/D_0$, was about 70%.

The same process was applied for the "package" of 100 non-anodized foils.

It was expected that during annealing the thin film formed on the surface of anodized foil would be transformed to the oxide layer. The purpose of the subsequent hot-rolling was twofold: 1) to crunch the oxide layer and to embed oxide particles into the aluminum matrix; 2) to enable the stable and strong interconnection and bonding between alternately arranged pure aluminum foils and those with oxide layers.

In both materials (A and NA), in the form of sheet approximately 4 mm wide, hot-rolling induced strong mutual bonding of foils, i.e., obtained multi layer material was compact and sound, with relatively straight and non-ragged edges, without peeling of the surface (Fig. 1).

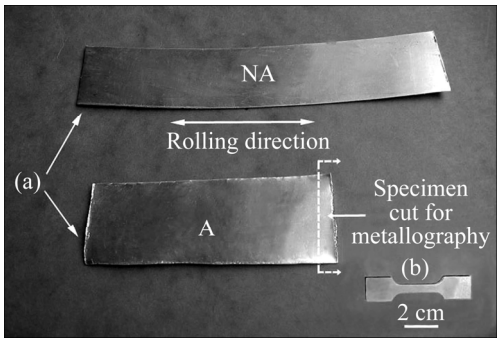

Fig. 1 Two different compact multilayer composite sheets after final hot-rolling: (a) Composite obtained from non-anodized foils (NA) and composite obtained from alternately arranged anodized and non-anodized foils (A); (b) Tensile test specimen

2.2 Metallographic preparation

Specimens (cut as shown in Fig. 1) were mounted in epoxy resin and prepared according to standard metallographic technique, i.e., ground with abrasive papers up to 2000 grit and polished with 3 μm diamond suspension. Specimens for optical microscopy were etched for 3 min in a mixture of 100 mL H_3PO_4 and 90 mL H_2SO_4.

2.3 Investigation of microstructure and mechanical properties

Optical microscope of type Zeiss Axiovert 25 and scanning electron microscope (SEM) of type JEOL Camscan FEG30 equipped with energy dispersive X-ray spectrometer (EDS) were used for microstructural characterization. The presence of phases in the material was detected by an X-ray diffractometer of type Siemens D500 using Cu K_α radiation (λ=0.15406 nm). The data were collected at room temperature with a 2θ range from 10° to 100° with a step size and scan rate of 0.02 (°)/s and 0.01 (°)/s, respectively. An intersection method applied on at least 10 SEM photomicrographs was used to measure dimensions of particles formed in the matrix of A composite.

A universal Instron TT-CM-L testing machine was used for room temperature tensile tests at strain rate of 1.3×10^{-3} s^{-1}. ASTM D 1708 micro-tensile specimens with the gauge length l=25mm, width b=4 mm and thickness d=0.7 mm, were used for tensile tests (Fig. 1(b)). Three point flexural tests were carried out on Instron machine with applied load of 1 kN and a loading speed of 0.01 cm/s. The dimensions of specimens were l=3 mm, b=20 mm and d=0.7 mm. For the sake of comparison, the specimen of pure aluminum with same dimensions was also subjected to flexural tests. Vickers hardness tests were performed using Carl Frank GmbH hardness tester with applying load of 20 N, whereas the time of indentation was 20 s. Results of hardness, tensile and flexural tests represent the average values of at least five measurements.

After tensile and flexural tests fracture surfaces of specimens were examined by SEM of type JEOL JSM 5800LV.

3 Results and discussion

3.1 X-ray diffraction analysis

X-ray diffraction (XRD) patterns of foils and multilayer composites are shown in Figs. 2(a)−(d).

XRD patterns of a pure aluminum foil show only the presence of aluminum peaks (Fig. 2(a)). Together with aluminum peaks in XRD patterns of NA composite, peaks of $Al(OH)_3$(s) also appear (Fig. 2(b)). At temperature of hot-rolling and in the presence of water vapor from the air formation of $Al(OH)_3$ is the result of the reaction:

$$2Al+6H_2O\longrightarrow 2Al(OH)_3(s)+3H_2(g) \quad (1)$$

The thin white-colored layer on aluminum foil after anodization corresponds to $Al_2(SO_4)_3$(s) (Fig. 2(c)), which was formed according to the reaction:

$$2Al+3H_2SO_4\longrightarrow Al_2(SO_4)_3(s)+3H_2(g) \quad (2)$$

After the final hot-rolling besides aluminum peaks, and remaining $Al_2(SO_4)_3$(s) peaks, peaks of low intensity corresponding to Al_2O_3 may be seen in XRD patterns of multilayer A composite (Fig. 2(d)). At 500 °C in the presence of water vapor $Al_2(SO_4)_3$(s) dissociates according to

$$Al_2(SO_4)_3(s)+6H_2O\longrightarrow 2Al(OH)_3(s)+3H_2SO_4 \quad (3)$$

Many metal hydroxides undergo thermal decomposition to produce the metal oxide and water [42]. For example, during hot-rolling at 500 °C $Al(OH)_3$(s) from Eq. (3) will decompose forming Al_2O_3(s):

$$2Al(OH)_3(s)\longrightarrow Al_2O_3(s)+3H_2O \quad (4)$$

In any case, the presence of Al_2O_3 was detected in the multilayer composite obtained by alternately arranged pure aluminum foils and those previously anodized. The main "source" for Al_2O_3 formation was obviously a solid compound $Al_2(SO_4)_3$. According to Ref. [43], the amounts of Al_2O_3 obtained from calcination of $Al_2(SO_4)_3$ at 400 and 600 °C are 12.31% and 16.31% (mass fraction), respectively.

3.2 Optical microscopy

Figure 3 shows the microstructure of the multilayer composites with final thickness of 0.7 mm. The boundaries between the individual foils which are not noticed in polished condition are discovered only after etching. It can be seen that good bonding occurs between foils and no gaps and pores are observed in interconnecting spaces (Figs. 3(a) and (b)). At higher magnification, a few coarser particles may be seen at

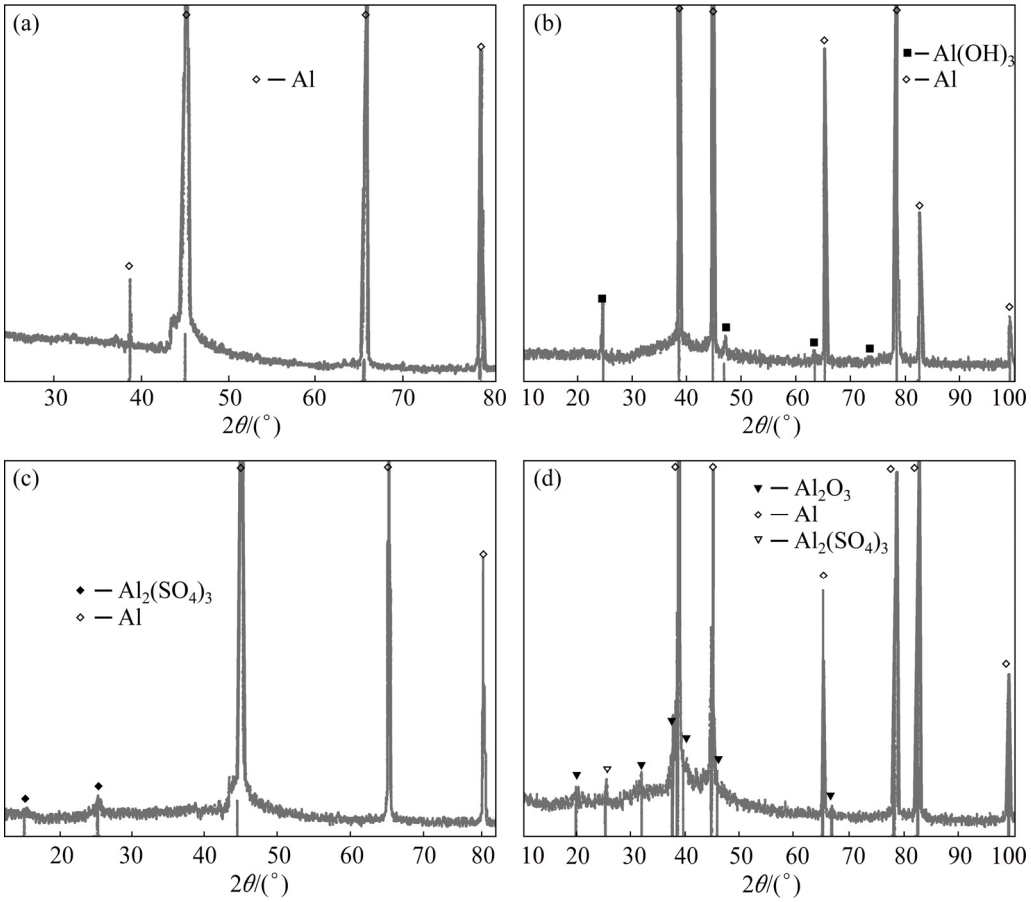

Fig. 2 XRD patterns: (a) Pure aluminum foil; (b) NA composite after hot-rolling at 500 °C for 1 h; (c) Aluminum foil after anodization; (d) A composite after hot-rolling at 500 °C for 1 h

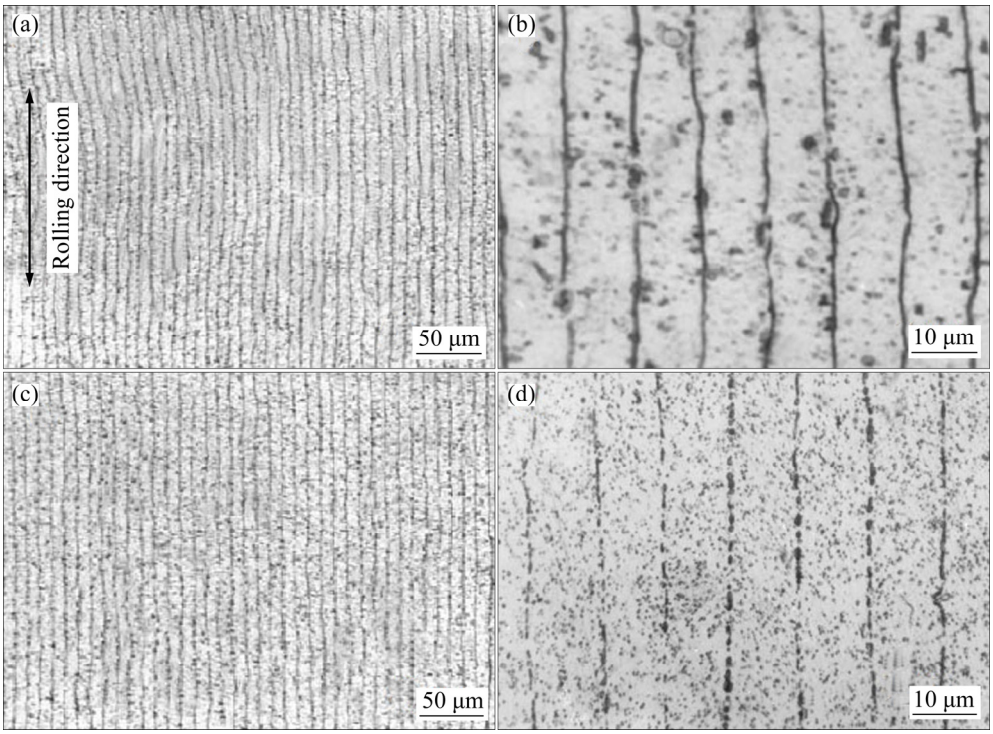

Fig. 3 Optical micrographs of multilayer composites after hot-rolling at 500 °C for 1 h: (a, b) NA composite; (c, d) A composite

boundaries between foils of NA composite (Fig. 3(b)). To the contrary, the boundaries between foils of A composite consist of a rod-like particles arranged in series of interrupted parallel rows (Fig. 3(d)). The tiny dark globules are distributed over the entire matrix of both composites, but their density is much higher in the matrix of A composite.

3.3 SEM and EDS analysis

SEM microstructures of NA composite with corresponding EDS are shown in Fig. 4. The boundaries between foils may be clearly seen, except when their appearance is sporadically disrupted (Fig. 4(a)). Black globules (Fig. 4(a)) may be either the result of over-etching or they represent the locations with particles pulled out during the previous metallographic preparation. A small rupture at the boundary between two foils may be seen (Fig. 4(b)). Change of the chemical composition along the line L shows that an increase of oxygen content clearly appears when the line crosses a particle at the boundary between two single foils, whereas at the same spot the decrease of aluminum content occurs. The maximum content of sulfur, although relatively low, corresponds to oxygen peak (Fig. 4(c)). In addition, when the line L crosses the white spot, a rather little increase of oxygen content is accompanied with the slight decrease of aluminum content. Similarly, when the line L crosses two particles formed on neighboring boundaries, the chemical composition changes, i.e., the content of oxygen increases, with the opposite effect occurring with aluminum. The maximal contents of sulfur appear at spots corresponding to oxygen (Fig. 4(d)). Oxygen contents are rather low and do not exceed 10% (molar fraction). The appearance of sulfur, with contents varying between 2% and 4% (molar fraction) at peaks, may be explained considering that H_2SO_4 is one of the components of etching mixture. It has to be added that these values should be regarded only as qualitative. Maximum and minimum peaks of oxygen and aluminum, respectively, suggest that a small amount of a solid phase, probably Al_2O_3, is formed at the boundaries between foils. The appearance of small amount of Al_2O_3 is the result of a few factors. First of all, the formation of a protective very thin oxide film present on the surface of the aluminum-based alloys should not be ignored. On the other side, based on Eqs. (1) and (4), it could be expected that small amount of Al_2O_3 will be also formed after the final hot-rolling of NA composite at 500 °C. However, the presence of Al_2O_3 has not been detected in XRD pattern of NA composite either due to the small amount of Al_2O_3 or the low detection limit of this instrument (Fig. 2(b)).

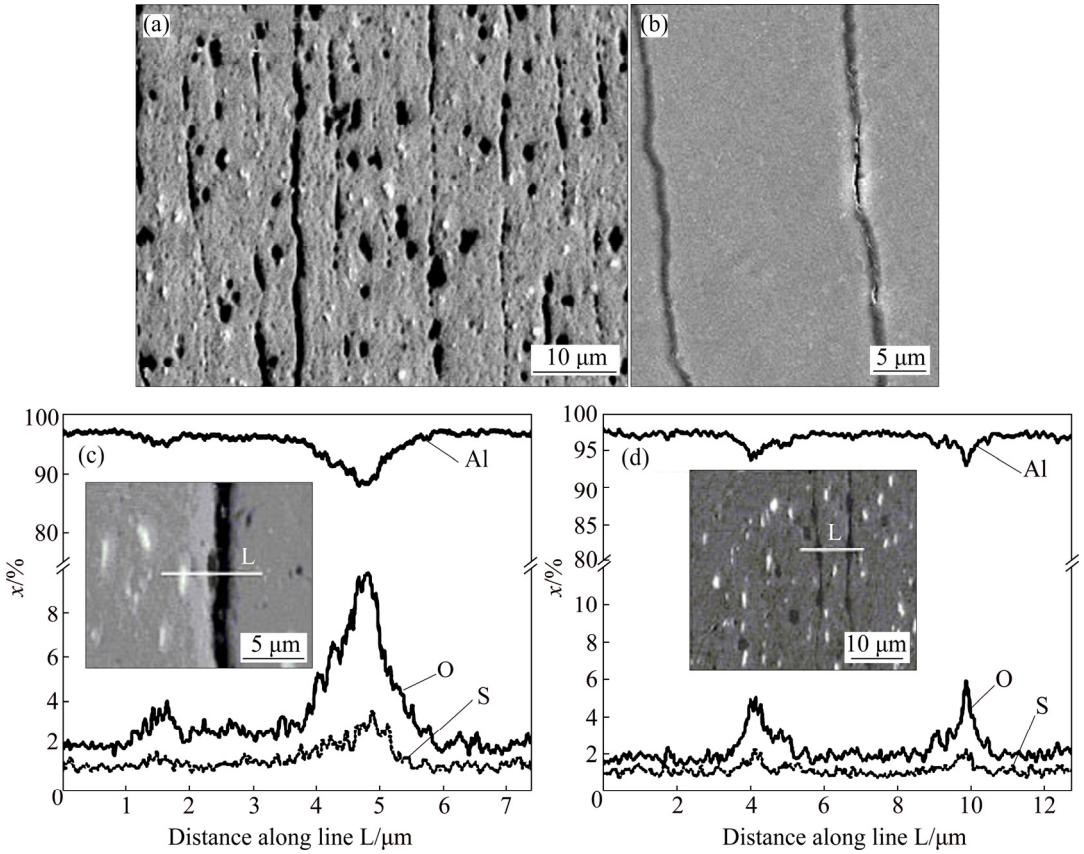

Fig. 4 SEM micrographs of NA composite after final hot-rolling: (a, b) SEM images; (c, d) SEM microstructures with corresponding EDS concentration lines along single boundary between two foils and along two adjacent boundaries, respectively

SEM images of A composite together with the change of chemical composition along the line L are shown in Fig. 5. Rod-like particles are arranged as a chain-like structure (Figs. 5(a) and (b)), and based on Fig. 3(d), it is supposed that they are mostly formed on boundaries between foils. Approximately, the length and width of these particles vary between 20 and 100 μm, and 3 and 10 μm, respectively. Particles of the same morphology, but significantly smaller are formed right next to the both edges of the specimen (Fig. 5(a)). Some particles were pulled out from the matrix surface (denoted by arrows) which probably occurred during metallographic preparation (Fig. 5(b)). The previously described "rods" are probably side planes of plate-like Al_2O_3 particles. Namely, in the longitudinal plane, these particles are seen as "rods" as they are broken by rolling along the rolling direction. However, these "rods" are fractions of much larger plate-like particles embedded in the interface between two adjacent aluminum foils [44], and according to these facts, "rods" will be designated as plates in the following text. Change of chemical composition along the line L shows the abrupt decrease of aluminum and steep increase of oxygen at locations when the line L crosses over three parallel plate-like particles (Fig. 5(c)). At their maxima and minima, the amount of oxygen and aluminum varies between 30% and 35%, and approximately 60% (molar fraction), respectively. These values are much higher if compared to corresponding amounts of oxygen and aluminum in NA composite (see Figs. 4(c) and (d)). The amount of sulfur is also higher (up to 10%, molar fraction) than in NA composite, which is the result of the previous anodization in diluted H_2SO_4, and disintegration of $Al_2(SO_4)_3$(s) at 500 °C. According to these results, it is reasonable to suppose that these plate-like particles are formed according to Eqs. (3) and (4). The molar fractions of aluminum and oxygen in Al_2O_3 calculated by a simple formula [45] are 63% and 37%, respectively. These results are very well matched with the chemical composition of plate-like particles in Fig. 5(c).

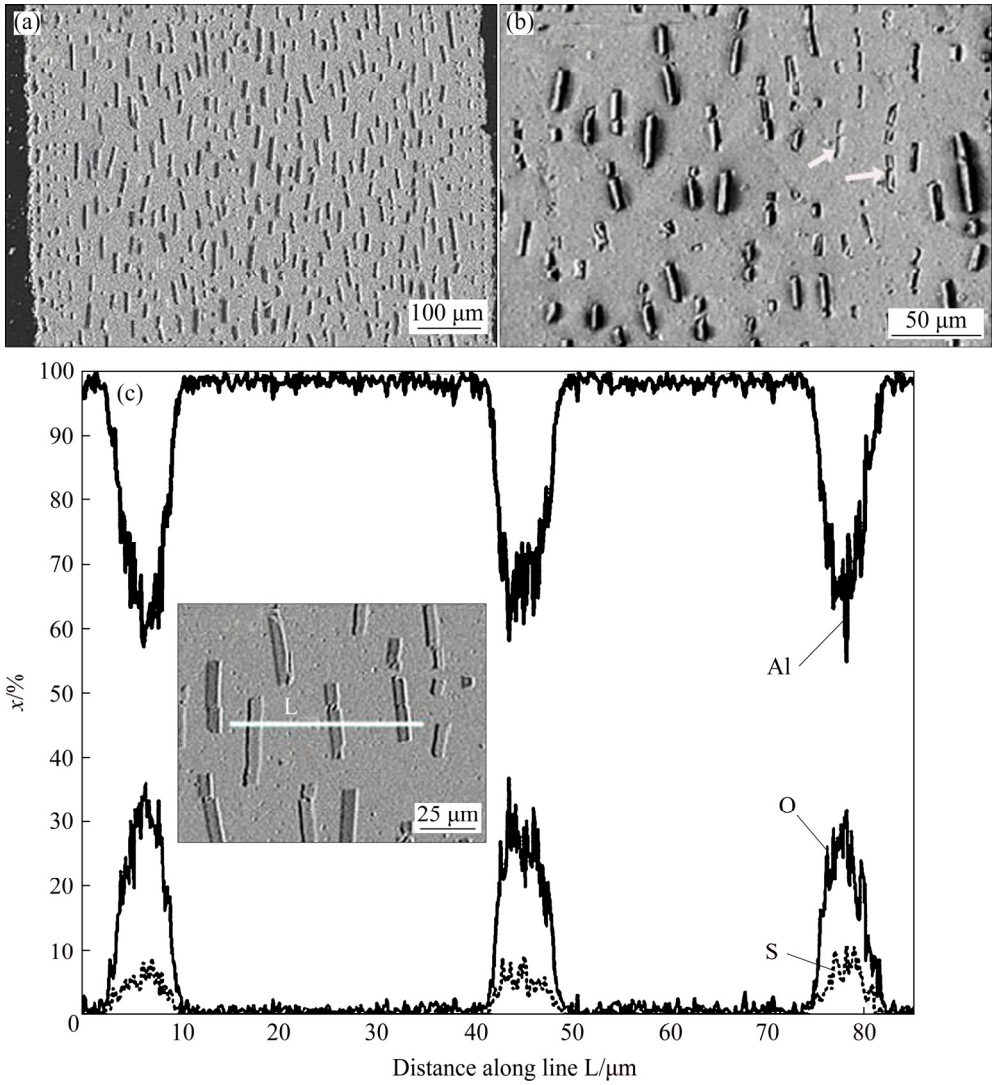

Fig. 5 SEM images of A composite after final hot-rolling: (a, b) SEM images; (c) SEM image with corresponding EDS along line L connecting three adjacent plate-like particles (Pulled-out particles are denoted by arrows)

Accompanied with XRD pattern (Fig. 2(d)), these results clearly indicate that the chemical composition of plate-like particles corresponds to Al_2O_3 in A composite.

To resolve the identification of black globules and white particles which appear in both NA and A composites, and plate-like particles present only in the matrix of A composite, a spot EDS analysis was performed. Due to rather small particles, SEM microstructures of these particles with their corresponding EDS spectra are presented in Fig. 6, whereas chemical compositions are given in Table 1. To obtain quantitative results of the chemical composition of small-sized particles and taking into account the relationship between the radius of the electronic EDS beam and the particles size, statistical study of many particles has been performed applying technique. Particles were analyzed by EDS in such a way that particles of the same morphology and the same level of darkness were chosen, and EDS analysis was performed at 3−10 different positions on each type of the particle. For this purpose, EDS point analysis was used.

The white particle contains aluminum in large excess and small amount of other alloying elements (Fig. 6(a)). However, content of alloying elements is higher in the dark particle (Fig. 6(b)). The results of several references [46−48] revealed that the dark particles in the matrix of alloy 8011 were intermetallic α-AlFeSi (Al_8Fe_2Si) phase, whereas the white particles

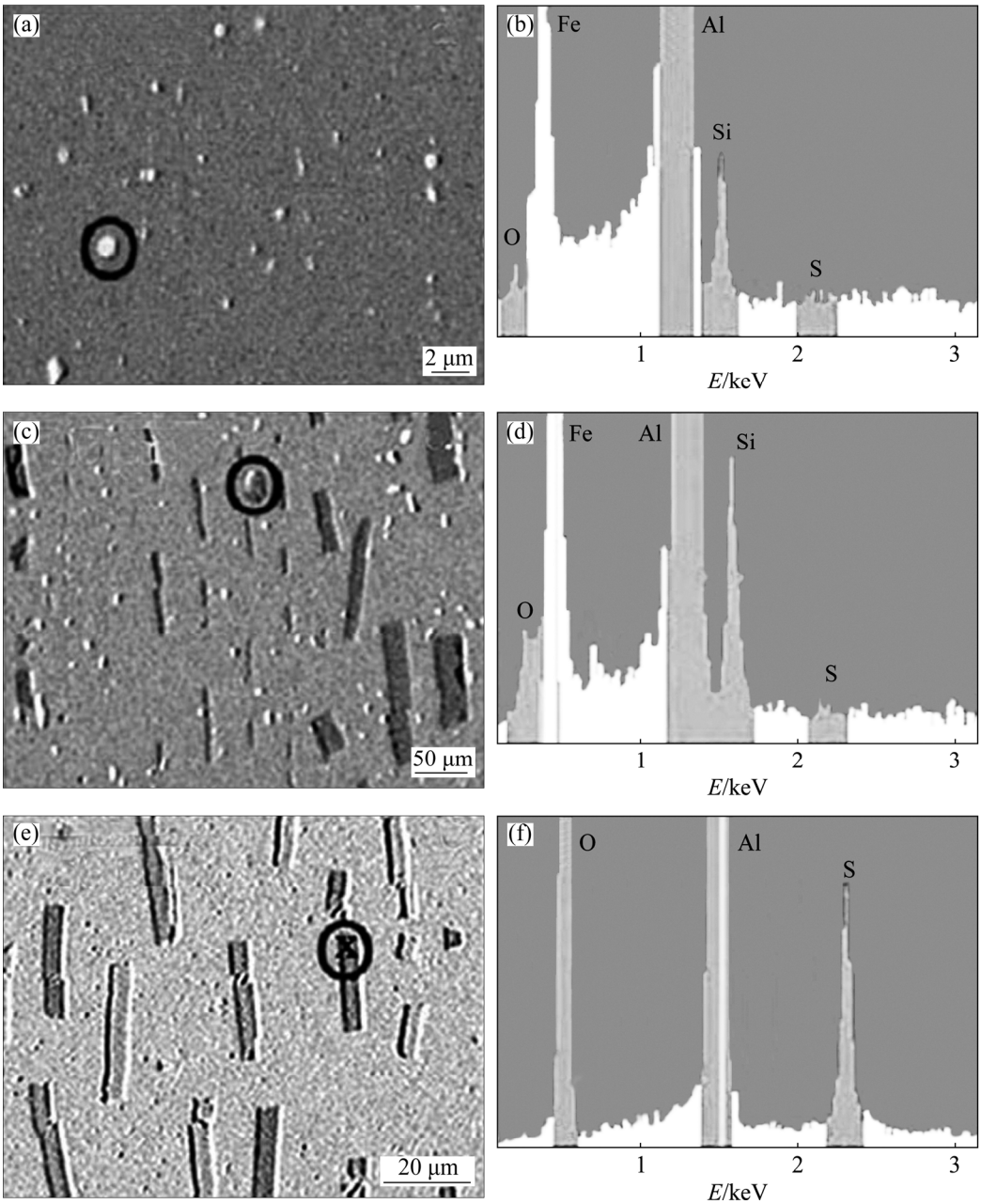

Fig. 6 SEM images and corresponding EDS spectra of particles in matrix of multilayer composites: (a, b) White globular particle; (c, b) Dark globular particle; (e, f) Plate-like particle

were identified as silicon-rich particles. Except for the content of oxygen, the chemical composition of dark particles is rather similar to the composition of particles defined as α-AlFeSi intermetallic phase in the matrix of 8011 alloy [46]. On the other side, the chemical composition of white particle from this work does not fit into the literature results [47]. The highest content of aluminum and oxygen was detected in plate-like particle (Fig. 6(c) and Table 1). This content is very similar to that measured along the line L (Fig. 5(c)). Sulfur may be always found in A composite, although somewhat less amount of sulfur was detected by spot analysis than along the line L. In any case, this result confirms previous findings that the chemical composition of plate-like particles corresponds to Al_2O_3.

3.4 Mechanical properties

Figure 7 illustrates the load−displacement plots obtained during flexural tests of A and NA composites. The characteristic of these curves was bending stiffness to peak load, much higher for A composite, due to no delamination observed and no oscillations before peak load. The curves can be divided into two regions. The first region, mostly linear in appearance, can be explained by the elastic deformation of both composites. The second region occurs after the load reached a peak value, when a significant load drop of about 55% of the peak load in the load−displacement curve was observed in A composite. This drop which is associated with both delamination and the fracture of Al_2O_3 plate-like particles suggests the brittle behavior of A composite, while the drop of the load curve of NA composite is under much subdued angle, suggesting that the process of delamination is very slow.

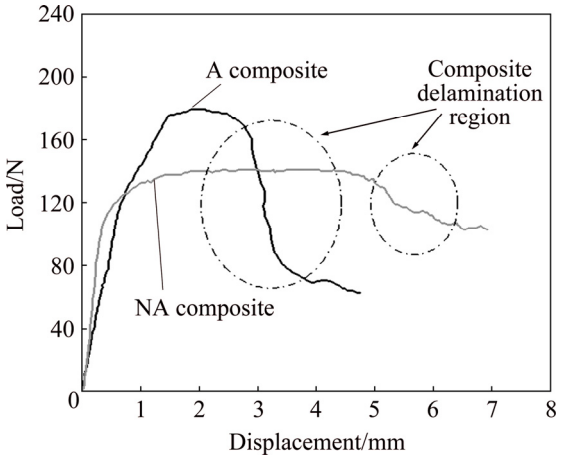

Fig. 7 Three-point flexural test showing load vs displacement plot of A and NA composites (Circles correspond to delamination region)

Mechanical properties of multilayer composites are listed in Table 2. The results show that the values of strength, hardness and elastic modulus of both NA and A composites are several times higher than those of the pure aluminum. However, the ductility of the composites is significantly lower. In addition, the same applies if

Table 1 Chemical analysis result of different particles in microstructure of A multilayer composite

Particle	*x*/%					
	O	Al	S	Si	Mn	Fe
White particle	1.5±1	94±3	0.03±0.02	1.7±0.5	0.05±0.01	2.5±0.6
Dark particle	6±1	78.5±2	0.25±0.02	5±1	0.9±0.1	9.4±0.3
Plate-like particle	32±5	65±3	3±1	–	–	–

EDS results given as mean values

Table 2 Mechanical properties of NA and A composites

Mechanical property	Commercial 8011 Al sheet (Temper O)	"Package" of 100 non-anodized foils (NA composite)	"Package" of 50 anodized and 50 non-anodized foils (A composite)
Hardness (HV_2)	25*	50	60
Yield strength, $\sigma_{0.2}$/MPa	36*	90	135
Ultimate tensile strength, σ_T/MPa	110*	115	170
Elongation, ε/%	34*	4	2.5
Modulus of elasticity**, E/GPa	71**	75	85
Maximum load at deflection/N	85	142	180
Maximum deflection, N/mm	8.5	4.2	2.0
Ultimate flexural strength, σ_f/MPa	124	435	560

* From Ref. [49]; ** Modulus of elasticity was experimentally determined from tangent to linear portion of slope of a stress−strain curve created during tensile tests

these properties are compared between NA and A composites: A composite, i.e., the "package" of 50 anodized and 50 non-anodized foils, exhibits higher strength, hardness and elastic modulus than composite NA, "package" of 100 non-anodized foils. Ductility of NA composite is 1.6 time higher than that of A composite.

An attempt was made to calculate modulus of elasticity of A composite and to compare calculated value with that experimentally obtained. There are several equations in the literature which may be used for comparison of the experimentally obtained modulus of elasticity of the multilayer composites with the theoretical value. KARAM's equation [50] is based on the simple rule of mixture, whereas HALPIN [51] introduced in his equation more parameters that can affect the value of modulus of elasticity:

$$E_{\mathrm{MMC}}=\frac{\left(1+\xi\eta V_{\mathrm{f}}\right)}{\left(1+\eta V_{\mathrm{f}}\right)}E_{\mathrm{M}} \tag{5}$$

where E_{MMC} is the modulus of elasticity of composite; E_{M} is the modulus of elasticity of the matrix, Al; V_{f} is the volume fraction of reinforcing particles.

Parameters η and ξ are defined by Eqs. (6) and (7), respectively,

$$\eta=\frac{\left(\frac{E_{\mathrm{f}}}{E_{\mathrm{M}}}-1\right)}{\left(\frac{E_{\mathrm{f}}}{E_{\mathrm{M}}}+\xi\right)} \tag{6}$$

$$\xi=2\frac{l}{d} \tag{7}$$

where E_{f} is the modulus of elasticity of reinforcing particles, Al_2O_3; l is the length of the particle; d is the diameter of the reinforcing particle.

Applying intersection method to measure dimensions of 300 particles, the following average results were obtained: l=50 μm, d=5 μm, whereas V_{f}=0.1. According to the literature data [52], E_{Al}=62 GPa, and $E_{\mathrm{Al_2O_3}}$=220 GPa. By calculating Eqs. (6) and (7) and replacing the relevant results in Eq. (5) gives the value E_{MMC}=76.5 GPa. Comparing this result with that in Table 2, the value of 76.5 GPa is nearly the same as that experimentally obtained for NA composite, i.e., the "package" of 100 non-anodized foils. The difference (10%) between the calculated value and 85 GPa can only be attributed to the insufficient measuring accuracy of values l, d and V_{f}, the main parameters of Eq. (5).

The appearance of specimens after three point flexural tests is shown in Fig. 8. It may be seen that only Specimen A was fractured during the test.

For calculation of the maximum flexural strength, σ_{f}, for a rectangular cross section, the following expression is used:

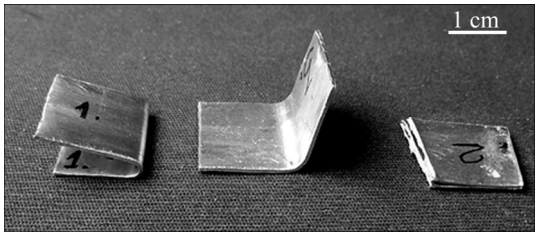

Fig. 8 Pure aluminum and multilayer NA and A composites after three-point flexural tests

$$\sigma_{\mathrm{f}}=\frac{3FL}{2bd^2} \tag{8}$$

where F is the maximum axial load (force) in N; L is the length of the support span in mm; b is the width of the specimen in mm; d is the the thickness of the specimen in mm.

Concerning three point flexural tests, the flexural strength would be the same as the tensile strength if the material is homogeneous. However, in many cases, this is not the case [53]. In fact, in non-homogeneous materials such as composites, flexural strength depends on properties of present defects, phases formed in the matrix, fibers, precipitates, inclusions, etc. Therefore, it is common for flexural strength to be higher than tensile strength for the same material. Values of flexural strength and tensile strength of pure aluminum are similar, but values of flexural strength of both NA and A composites are much higher than tensile strength of corresponding composites. Also, the maximum load at deflection and ultimate flexural strength behave in the same way as previously described mechanical properties, i.e., according to the rising sequence: pure Al→NA composite → A composite. The opposite situation is when deflection is concerned.

According to the results presented in Table 2, it is unambiguously clear that multilayer composites possess hardness, tensile and flexural strength higher than pure aluminum. Exception is ductility which decreases with increasing strength. Densely packed and arranged at a short distance, boundaries between foils represent obstacles to dislocation motion thus contributing to the strengthening of the matrix. Additional factors contributing to the unexpectedly large values of flexural strength could be ascribed to the strengthening effect of Al_2O_3 plate-like particles and the friction forces imposed by these particles to the aluminum matrix during flexural tests. Thus, hardness, tensile and flexural strength, as well as modulus of elasticity of composite A are superior compared to corresponding properties of two other materials investigated in this work.

3.5 Fracture morphology

Fracture surface morphologies of multilayer composites after tensile tests are shown in Fig. 9.

The microfractographs of NA composite after tensile test show dimples which indicate the microvoid coalescence mechanism of ductile fracture (Figs. 9(a) and (b)). A dual dimple size may be observed in the matrix. Majority of dimples are stretched elliptic, suggesting that the fracture is affected by shear stresses. These micrographs show that the failure mode was shear ductile fracture. Two parallel cracks at a distance of approximately 20 μm, which may be seen at higher magnification (marked with arrows in Fig. 9(b)), probably correspond to the insufficient connection between two pure aluminum foils which lead to the appearance of rupture.

It is known that fracture in metal matrix composites is governed by three different mechanisms [54]. These mechanisms are fracture of reinforcing particles, detachment of interface and nucleation and growth of dimples. The big difference in elastic moduli of the matrix and reinforcing particle may produce the local stress concentration near or around the reinforcing particle. At some extent, this concentration reaches the critical value, causing the fracture of the reinforcing particle and separation of matrix ligaments from the fractured particles. Such a situation occurred during tensile test of A composite (Figs. 9(c) and (d)). Al_2O_3 plate-like particles (P) are embedded in the parallel rows in aluminum matrix, and a few shallow dimples (D) may also be seen (Fig. 8(c)). Parallel rows of plate-like and cracked plate-like particles (CP) are separated by ductile matrix ligament L (Fig. 9(d)). Rectangular hole (H) with regular shape is the original site where the plate-like particle was pulled out from the matrix. The fracture failure of A composite is mostly brittle due to decohesion of Al_2O_3 plate-like particles in the interface with some presence of ductile fracture of aluminum ligaments.

Fracture surface morphologies of multilayer A composite after three point flexural tests are shown in Fig. 10.

Fracture modes after flexural tests are rather difficult to define and resolve and due to their non-characteristic appearance they can hardly be classified into any of existing modes. The general morphology of the fracture is that the regular arrangement of foils was completely disrupted and destroyed during the test. Parts of single foils (F) with the uneven surface (FS) may be clearly seen (Fig. 10(a)), whereas a row of wrinkled foils exists between bundles of foils (BF) (Fig. 10(b)). At higher magnification, bundles of foils (BF), showing presence of dimples, are interrupted by Al_2O_3 plate-like particles (P) (Fig. 10(c)). At even higher magnification, delamination and sporadic fracture of plate-like particles (P) may be clearly seen (Fig. 10(d)). The fracture mode after flexural tests of A composite must be due to delamination of Al_2O_3 platelets combined with the ductile fracture of aluminum ligaments.

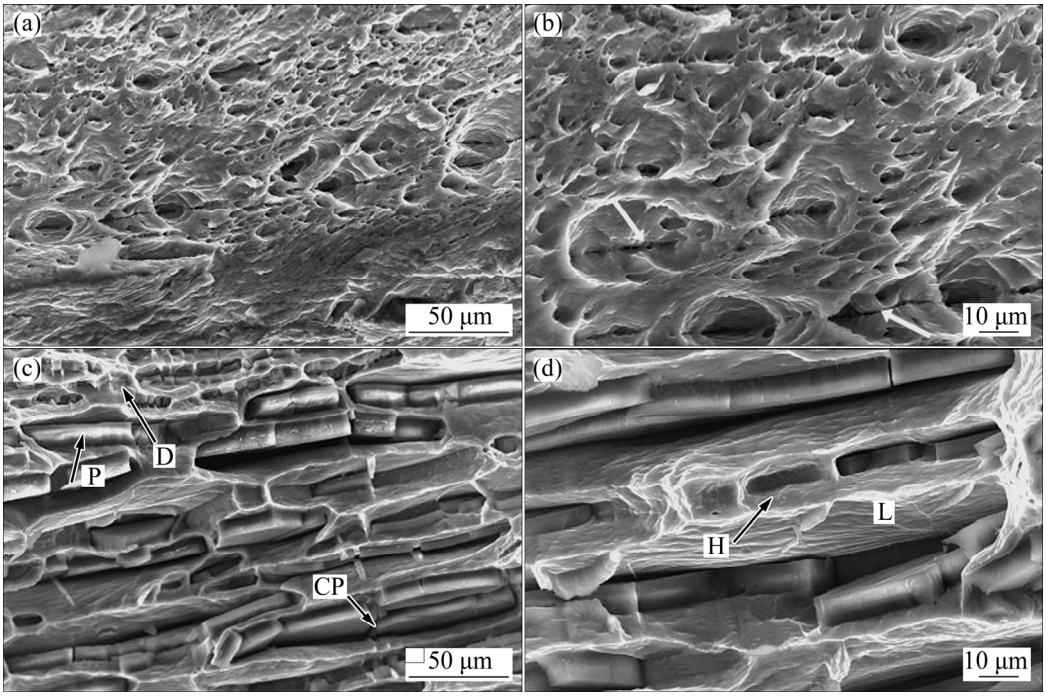

Fig. 9 SEM images of fracture surfaces after tensile tests: (a, b) NA composite; (c, d) A composite (D—Dimple; P—Plate-like particle; CP—Cracked plate-like particle; L—Matrix ligament; H—Hole)

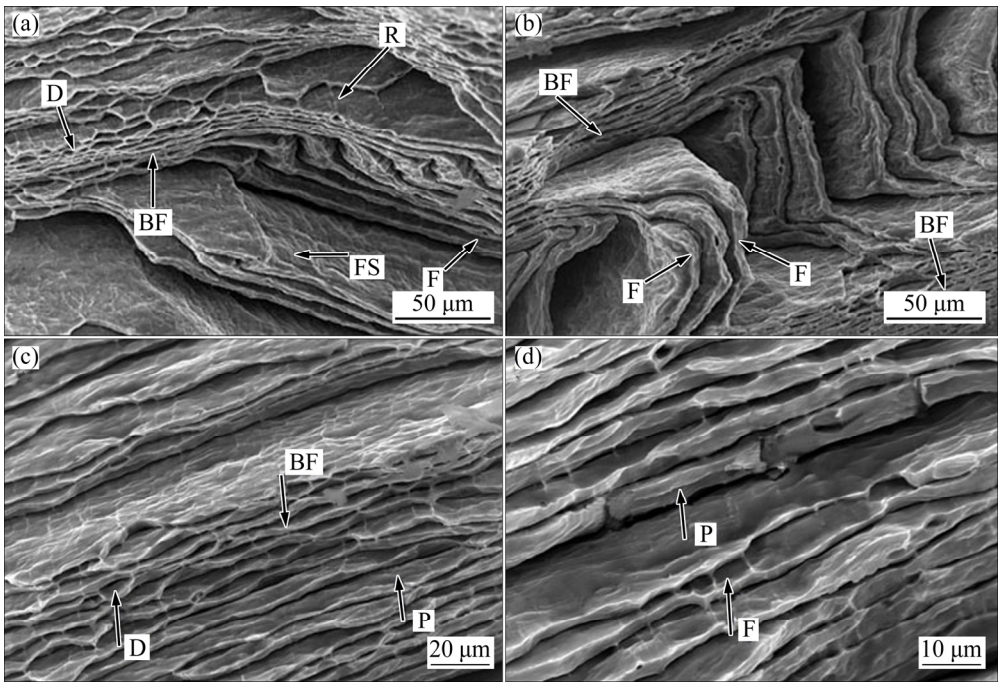

Fig. 10 SEM images of A composite fracture surfaces after three-point flexural tests (D—Dimples; R—River markings; BF—Bundle of foils; F—Single foil; FS—Foil surface; P—Plate-like particles)

4 Conclusions

1) 50 anodized and 50 non-anodized household commercial aluminum foils (17 μm thick) were alternately packed (composite A). Hot-rolling at 500 °C was applied in the final process with the total amount of hot deformation of about 70%. Another "package" of 100 non-anodized foils was also prepared (composite NA) in the same way. In both materials (A and NA) hot-rolling induced strong mutual bonding of foils, i.e., obtained multilayer material was compact and sound.

2) Microstructural characterization confirmed that the plate-like particles distributing in parallel rows in the aluminum matrix of A composite correspond to Al_2O_3. Also, maximum and minimum peaks of oxygen and aluminum, respectively, suggest that after the final hot-rolling of NA composite, a small amount of coarser particles were formed at boundaries between foils.

3) Values of strength, hardness and elastic modulus of both NA and A composites are several times higher than those of the pure aluminum. However, the ductility of composites is significantly lower. In the same time, the "package" of 50 anodized and 50 non-anodized foils, exhibits higher strength, hardness and elastic modulus than NA composite, the "package" of 100 non-anodized foils. Ductility of NA composite is 1.6 times higher than that of A composite.

4) An attempt was made to calculate modulus of elasticity of A composite and to compare it with experimentally obtained value. A fairly good agreement (the difference was 10%) of experimental (85 GPa) and calculated (76.5 GPa) values was obtained.

5) Maximum load at deflection and ultimate flexural strength behave in the same way as tensile properties, i.e., according to the rising sequence: pure Al→NA composite → A composite. The opposite situation is when deflection is concerned.

6) Fracture failure after tensile tests corresponds to the change of ductility, i.e., fracture surface of NA composite with higher ductility possesses characteristics of ductile fracture, whereas mostly brittle fracture prevails in fracture of less ductile A composite. The fracture mode after flexural tests of A composite must be due to delamination of Al_2O_3 platelets combined with the ductile fracture of the pure aluminum ligaments.

Acknowledgments

This work was financially supported by the Ministry of Education, Science and Technological Development of the Republic of Serbia through the Project Nos. III45012 and ON174004. Authors are grateful to Dr. M. Zrilic for the help in execution of three-point bending experiments.

References

[1] KAVARANA F H, RAVICHANDRAN K S, SAHAY S S. Nanoscale steel-brass multilayer laminates made by cold rolling: Microstructure and tensile properties [J]. Scripta Materialia, 2000, 42: 947−954.

[2] MISRA A, HIRTH J P, HOAGLAND R G. Length-scale-dependent deformation mechanisms in incoherent metallic multilayered composites [J]. Acta Materialia, 2005, 53: 4817−4824.

[3] GIGUERE A, HAI N H, DEMPSEY N, GIVORD D. Preparation of microstructured and nanostructured magnetic materials by mechanical deformation [J]. Journal of Magnetism and Magnetic Materials, 2002, 242−245: 581−584.

[4] HSIEH P J, HUNG Y P, HUANG J C. Transformation into nanocrystalline or amorphous materials in Zr−X binary systems using ARB route [J]. Scripta Materialia, 2003, 49: 173−178.

[5] Mc KEOWN J, MISRA A, KUNG H, HOAGLAND R G, NASTASI M. Microstructures and strength of nanoscale Cu−Ag multilayers [J]. Scripta Materialia, 2002, 46: 593−698.

[6] WADLEY H N G, HSIUNG L M, LANKEY R L. Artificially layered nanocomposites fabricated by jet vapor deposition [J]. 1995, 5: 935−940.

[7] NABI RAHNI D M A, TANG P T, LEISNER P. The electrolytic plating of compositionally modulated alloys and laminated metal nano-structures based on an automated computer-controlled dual-bath system [J]. Nanotechnology, 1996, 7: 134−143.

[8] KRONE W C, YAHYA A N, PEREPEZKO J H. Bulk shape memory NiTi with refined grain size synthesized by mechanical alloying [J]. Materials Science Forum, 2002, 386−388: 597−602.

[9] BATTEZZATI L, ANTONIONE C, FRACCHIA F. Ni−Al intermetallics produced by cold-rolling elemental sheets [J]. Intermetallics, 1995, 3: 67−71.

[10] HAI N H, DEMPSEY N M, GIVORD D. Hard magnetic Fe−Pt alloys prepared by cold-deformation [J]. Journal of Magnetism and Magnetic Materials, 2003, 262: 353−360.

[11] YANG D, CIZEK P, HODGSON P, WEN C E. Ultrafine equiaxed-grain Ti/Al composite produced by accumulative roll bonding [J]. Scripta Materialia, 2010, 62: 321−324.

[12] ZHANG R, ACOFF V L. Processing sheet materials by accumulative roll bonding and reaction annealing from Ti/Al/Nb elemental foils [J]. Materials Science and Engineering A, 2007, 463: 67−73.

[13] OHSAKI S, KATO S, TSUJI N, OHKUBO T, HONO K. Bulk mechanical alloying of Cu−Ag and Cu/Zr two-phase microstructures by accumulative roll-bonding process [J]. Acta Materialia, 2007, 55: 2885−2895.

[14] SAITO Y, UTSUNOMIYA H, TSUJ N, SAKAI T. Novel ultra-high straining process for bulk materials-development of the accumulative roll-bonding (ARB) process [J]. Acta Materialia, 1999, 47: 579−583.

[15] WILLIAMS J C, STARKE E A Jr. Progress in structural materials for aerospace systems [J]. Acta Materialia, 2003, 51: 5775−5799.

[16] EVANCHO J W, KAUFMAN J G. New 6XXX-series alloys for auto body sheet [J]. Aluminum, 1977, 53: 609−613.

[17] ALTENPOHL D G. Aluminum technology, applications, and environment: A profile of a modern metal [M]. 6th ed. Washington, D.C.: Aluminium Association, Minerals, Metals & Materials Society (TMS), 1998.

[18] REIHANIAN M, BAGHERPOUR E, PAYDAR M H. Particle distribution in metal matrix composites fabricated by accumulative roll bonding [J]. Materials Science and Technology, 2012, 28: 103−108.

[19] LI X B, ZU G Y, WANG P. High strain rate tensile performance and microstructural evolution of Al/Cu laminated composite under dynamic loading [J]. Materials Science and Engineering A, 2014, 612: 89−95.

[20] DEHSORKHI R N, QODS F, TAJALLY M. Investigation on microstructure and mechanical properties of Al−Zn composite during accumulative roll bonding (ARB) process [J]. Materials Science and Engineering A, 2011, 530: 63−72.

[21] DEHSORKHI R N, QODS F, TAJALLY M. Application of continual annealing and roll bonding (CAR) process for manufacturing Al−Zn multilayered composites [J]. Materials Science and Engineering A, 2012, 549: 206−212.

[22] HIDALGO P, CEPEDA-JIMÉNEZ C M, RUANO O A, CARREÑO F. Influence of the processing temperature on the microstructure, texture and hardness of the 7075 aluminium alloy fabricated by accumulative roll bonding [J]. Metallurgical and Materials Transactions A, 2010, 41: 758−767.

[23] MOZAFFARI A, DANESH MANESH H, JANGHORBAN K. Evaluation of mechanical properties and structure of multilayered Al/Ni composites produced by accumulative roll bonding (ARB) process [J]. Journal of Alloys and Compounds, 2010, 489: 103−109.

[24] CHANG H, ZHENG M Y, GAN W M, WU K, MAAWAD E, BROKMEIER H G. Texture evolution of the Mg/Al laminated composite fabricated by the accumulative roll bonding [J]. Scripta Materialia, 2009, 61: 717−720.

[25] CHEN M C, HSIEH H C, WU W. The evolution of microstructures and mechanical properties during accumulative roll bonding of Al/Mg composite [J]. Journal of Alloys and Compounds, 2006, 416: 169−172.

[26] WEI K X, WEI W, DU Q B, HU J. Microstructure and tensile properties of Al−Mn alloy processed by accumulative roll bonding [J]. Materials Science and Engineering A, 2009, 525: 55−59.

[27] YANG D, HODGSON P, WEN C. The kinetics of two-stage formation of $TiAl_3$ in multilayered Ti/Al foils prepared by accumulative roll bonding [J]. Intermetallics, 2009, 17: 727−732.

[28] XU L, CUI Y Y, HAO Y L, YANG R. Growth of intermetallic layer in multi-laminated Ti/Al diffusion couples [J]. Materials Science and Engineering A, 2006, 435−436: 638−647.

[29] IBRAHIM I, MOHAMED F, LAVERNIA E J. Particulate reinforced metal matrix composites: A review [J]. Journal of Material Science, 1991, 26: 1137−1156.

[30] CHIN E. Army focused research team on functionally graded armor composites [J]. Materials Science and Engineering A, 1999, 259: 155−161.

[31] TAHAMTAN S, HALVAEE A, EMAMY M, ZABIHI M S. Fabrication of Al/A206−Al_2O_3 nano/micro composite by combining ball milling and stir casting technology [J]. Materials and Design, 2013, 49: 347−359.

[32] CASATI R, VEDANI M. Metal matrix composites reinforced by nano-particles: A review [J]. Metals, 2014, 4: 65−83.

[33] PRASAD S V, ASTHANA R. Aluminum metal-matrix composites for automotive applications: tribological considerations [J]. Tribology Letters, 2004, 17: 445−453.

[34] LEE D W, KIM B K. Nanostructured Cu−Al_2O_3 composite produced by thermochemical process for electrode application [J]. Materials Letters, 2004, 58: 378−383.

[35] JAMAATI R, TOROGHINEJAD M R. Manufacturing of high-strength aluminum/alumina composite by accumulative roll bonding [J]. Materials Science and Engineering A, 2010, 527: 4146−4151.

[36] REZAYAT M, AKBARZADEH A, OWHADI A. Production of high strength Al−Al_2O_3 composite by accumulative roll bonding [J]. Composites: Part A, 2012, 43: 261−267.

[37] MEHR V Y, REZAEIAN A, TOROGHINEJAD M R. Mechanical properties and microstructure evolutions of multilayered Al−Cu composites produced by accumulative roll bonding process and subsequent annealing [J]. Materials Science and Engineering A, 2014, 601: 40−47.

[38] KAMALI ARDAKANI M R, AMIRKHANLOU S, KHORSAND S. Cross accumulative roll bonding—A novel mechanical technique for significant improvement of stir-cast Al/Al_2O_3 nano-composite properties [J]. Materials Science and Engineering A, 2014, 591: 144−148.

[39] ALIZADEH M, BENI H A, GHAFFARI M, AMINI R. Properties of high specific strength Al−4wt.%Al_2O_3/B_4C nano-composite produced by accumulative roll bonding process [J]. Materials and Design, 2013, 50: 427−432.

[40] ISLAMGALIEV R K, BUCHGRABER W, KOLOBOV Y R, AMIRKHANOV N M, SERGUEEVA A V, IVANOV K V, GRABOVETSKAYA G P. Deformation behavior of Cu-based nanocomposite processed by severe plastic deformation [J]. Materials Science and Engineering A, 2001, 319−321: 872−876.

[41] REZAYAT M, AKBARZADEH A. Deformation behavior of Cu-based nanocomposite processed by severe plastic deformation [J]. Material Science and Technology, 2012, 28: 1233−1240.

[42] GALWAY A K, BROWN M E. Thermal Decomposition of Ionic Solids [M]. Amsterdam, Netherlands: Elsevier Science, 1999.

[43] MATORI K A, WAH L C, HASHIM M, ISMAIL I, ZAID M H M. Phase transformations of α-alumina made from waste aluminum via a precipitation technique [J]. International Journal of Molecular Science, 2012, 13: 16812−16821.

[44] CEPEDA-JIMÉNEZ C M, POZUELOB M, GARCÍA-INFANTAA J M, RUANO O A, CARREÑO F. Influence of the alumina thickness at the interfaces on the fracture mechanisms of aluminium multilayer composites [J]. Materials Science and Engineering A, 2008, 496: 133−142.

[45] KHALIL A. How to convert atomic percent to weight percent and vice versa [EB/OL]. http://www.scribd.com/doc/74247139. 2017−01−25.

[46] KIM H W, KANG S B, TSUJI N, MINAMINO Y. Elongation increase in ultra-fine grained Al−Fe−Si alloy sheets [J]. Acta Materialia, 2005, 53: 1737−1749.

[47] XING Z P, KANG S B, KIM H V. Softening behavior of 8011 alloy produced by accumulative roll bonding process [J]. Scripta Materialia, 2001, 45: 597−604.

[48] MONDOLFO L F. Aluminum alloys: Structure and properties [M]. London, UK: Butterworths, 1976.

[49] 8011A-O aluminum [EB/OL]. http://www.makeitfrom.com/material-properties. 2017−01−25.

[50] KARAM G N. Effect of fibre volume on tensile properties of real unidirectional fibre-reinforced composites [J]. Composites, 1991, 22: 84−88.

[51] HALPIN J C. Stiffness and expansion estimates for oriented short fiber composites [J]. Journal of Composite Materials, 1969, 2: 732−734.

[52] Ceramic Source 1992-1993: Annual company directory and buyer's guide [M]. Columbus, OH, USA: The American Ceramic Society Inc, 1992.

[53] CALLISTER W D Jr, RETWISCH D G. Materials science and engineering: An introduction [M]. 8th ed. New York, NY, USA: John Wiley & Sons Inc, 2007.

[54] JAMAATI R, AMIRKHANLOU S, TOROGHINEJAD M R, NIROUMAND B. Effect of particle size on microstructure and mechanical properties of composites produced by ARB process [J]. Materials Science and Engineering A, 2011, 528: 2143−2148.

通过轧制纯铝箔和阳极铝箔制备多层铝基复合材料

Milan T. JOVANOVIĆ, Nenad ILIĆ, Ivana CVIJOVIĆ-ALAGIĆ, Vesna MAKSIMOVIĆ, Slavica ZEC

Department of Materials Science, Institute of Nuclear Sciences "Vinča",
University of Belgrade, P. O. Box 522, 11001 Belgrade, Serbia

摘　要：介绍了一种以商业纯铝箔为基体的多层复合材料的加工过程、组织结构和力学性能。采用热轧制交替排布的纯铝和阳极铝箔制备多层复合材料；此外，采用同样的工艺制备纯铝箔多层复合材料。在这两种情况下，均得到紧实致密的多层复合材料。为了研究复合材料的微观组织演变和力学性能，分别进行了光学和扫描电镜(SEM)、能谱(EDS)、X 射线衍射(XRD)分析以及硬度、拉伸和三点弯曲试验。微观组织表征显示，阳极铝复合材料铝基体中平行分布着棒状 Al_2O_3 颗粒，而且铝箔界面间生成少量粗大颗粒。两种复合材料的硬度、强度、弹性模量和抗弯强度均高于纯铝材料的，而延展性明显降低。与纯铝箔多层复合材料相比，阳极铝箔多层复合材料具有较高的强度和弹性模量以及较低的延展性。材料的断裂失效方式与延展性的变化一致。

关键词：铝箔；阳极氧化；多层复合材料；Al_2O_3 颗粒；强度；断裂

(Edited by Bing YANG)